



OPEN ACCESS

EDITED BY

Nissim Fraija,
National Autonomous University of
Mexico, Mexico

REVIEWED BY

José Domingo Arbañil Vela,
Universidad Privada del Norte, Peru
Rosa L. Becerra,
National Autonomous University of
Mexico, Mexico
Boris Betancourt Kamenetskaia,
Institute for Basic Science (IBS),
Republic of Korea

*CORRESPONDENCE

Gabriela Conde-Saavedra,
✉ gabriela.saavedra@inpe.br

RECEIVED 09 October 2025

REVISED 29 January 2026

ACCEPTED 05 February 2026

PUBLISHED 02 March 2026

CITATION

Conde-Saavedra G, Aguiar OD, de
Oliveira HP and Ujevic M (2026)
Studying the detectability of
gravitational waves from the
post-merger phase in binary neutron
star signals.
Front. Astron. Space Sci. 13:1721816.
doi: 10.3389/fspas.2026.1721816

COPYRIGHT

© 2026 Conde-Saavedra, Aguiar, de
Oliveira and Ujevic. This is an
open-access article distributed under
the terms of the [Creative Commons
Attribution License \(CC BY\)](https://creativecommons.org/licenses/by/4.0/). The use,
distribution or reproduction in other
forums is permitted, provided the
original author(s) and the copyright
owner(s) are credited and that the
original publication in this journal is
cited, in accordance with accepted
academic practice. No use, distribution
or reproduction is permitted which
does not comply with these terms.

Studying the detectability of gravitational waves from the post-merger phase in binary neutron star signals

Gabriela Conde-Saavedra^{1*}, Odylio D. Aguiar¹, H. P. de Oliveira²
and Maximiliano Ujevic³

¹Divisão de Astrofísica, Instituto Nacional de Pesquisas Espaciais, São José dos Campos, Brazil,
²Instituto de Física, Universidade do Estado do Rio de Janeiro, Rio de Janeiro, Brazil, ³Centro de
Ciências Naturais e Humanas, Universidade Federal do ABC, Santo André, Brazil

We study the detectability of next-generation gravitational wave detectors by analyzing 10 post-merger signals in binary neutron star simulations assuming they are sources located at $d=88$ Mpc and $d=159$ Mpc. The simulation characteristics are based on the binary parameters estimated for the GW190425 event. Our results show that the most optimistic result is given by the Cosmic Explorer detector at the highest values of the merger rate ($R_0 = 1700 \text{ Gpc}^{-3}\text{yr}^{-1}$) and signal-to-noise ratio ($\text{SNR}_{\text{high}} = 5.34 \pm 3.06$), providing $N = 1.44 \pm 2.48$ detections per year.

KEYWORDS

binary neutron star coalescences, BNS merger rate, next-generation detectors, number of detections, post-merger phase gravitational waves

1 Introduction

Binary neutron star (BNS) coalescences are sources for gravitational wave (GW) signals that have three characteristic phases: inspiral, merger, and post-merger (PM). During the inspiral, the GW amplitude and frequency increase as the stars spiral closer together, and the tidal deformability carries information about the neutron-star equation of state (EoS) in the signal (Abbott et al., 2017; 2018; Read et al., 2013). The merger phase is a transient stage in which the neutron stars actually collide, undergo strong deformations and tidal disruption, and generate shockwaves that heat matter, so the temperature rises even more just before the merger structure sets into a new remnant object (Hotokezaka et al., 2013; Kiuchi et al., 2015; Radice, 2020). Subsequently, the evolution of the remnant represents the post-merger phase by showing a damped oscillation-like GW signal at frequencies $f \geq 1$ kHz. The main frequency peak corresponds to the fundamental mode of oscillation of the remnant until it either collapses or stabilizes, so there is no longer emission of GW at the end. In the post-merger stage, the lifetime and composition of the remnant can be regulated by neutrino heating and viscosity (Perego et al., 2014; Radice et al., 2018). In addition, the post-merger stage outcome can yield a prompt-collapse black hole, a stable new neutron star, or a black hole with a previous formation of a hypermassive neutron star (HMNS) or a supermassive neutron star (SMNS), (Bauswein et al., 2013; Shibata et al., 2019; Dietrich et al., 2021). The final product of the coalescence depends on the total mass and the EoS model of the binary systems, then the maximum mass of a neutron star is key to define if the product is a neutron star or a black hole. The PM stage, besides determining the remnant type, it may provide information about the EoS according to

numerical relativity simulation studies (Takami et al., 2014) that have shown quasi-universal relations (Bernuzzi et al., 2014) between post-merger dominant peak frequencies with inspiral neutron star properties such as the radius, tidal deformability and compactness. Recent studies such as Puecher et al. (2023) used waveform models for the three stages and explored how the quasi-universal relations are able to extract the EoS information with gravitational wave detector networks, including advanced (Adv+) detectors and third generation (3G) observatories.

Regarding electromagnetic (EM) observations of neutron star masses, we can mention pulsars in binary systems or X-ray binaries (systems where the neutron star accretes matter from a companion producing intense X-ray emission (Özel and Freire, 2016)). Neutron star mass measurements are around $\approx 1.35 - 1.46 M_{\odot}$ (Thorsett and Chakrabarty, 1999; Zhang et al., 2011). Others, such as PSR J1614-2230 have higher masses around $1.97 \pm 0.04 M_{\odot}$ (Demorest et al., 2010)). Another example is PSR J0740 + 6620 with a mass of $\approx 2.14 M_{\odot}$ (Cromartie et al., 2019). These two objects set constraints on the maximum mass and on the EoS of dense matter. On the other hand, when gravitational wave detectors started operating, two BNS events were observed. GW170817 was the first, providing estimates of both masses in the range $\approx 1.17 - 1.60 M_{\odot}$, with a total mass of $\sim 2.74 M_{\odot}$ (Abbott et al., 2017). The precise values depended on the assumptions about the spin of the neutron star, that is, if one allows higher spins ($\chi \sim 0.89$), the credible intervals for the masses improve the uncertainty, while low spin values ($\chi \sim 0.05$) allowed better credible intervals for the estimated masses (Abbott et al., 2019). The second BNS event, GW190425, was reported with masses in the range $\approx 1.60 - 2.52 M_{\odot}$ and $\approx 1.12 - 1.68 M_{\odot}$, with a total mass of $\sim 3.4 M_{\odot}$ (Abbott B. P. et al., 2020). The component masses of the GW170817 event were found to be consistent with the EM measurements of Galactic BNS systems, while for the second event GW190425, the total mass values were unusual compared to EM observations. According to EM observations, compact objects apparently fall into two populations: neutron stars up to $\sim 2.14 M_{\odot}$ (Cromartie et al., 2019), and black holes starting at $\sim 5 M_{\odot}$ (Özel et al., 2010) or $3.3 M_{\odot}$ (Thompson et al., 2019). Then, the region in between ($2 - 5 M_{\odot}$) is called the “mass gap” (Farr et al., 2011). In the case of GW observations, GW190814 included a secondary component with a mass of $2.50 - 2.67 M_{\odot}$ (Abbott R. et al., 2020). More recently, GW230529 included a component of $\sim 3.6_{-1.2}^{+0.8} M_{\odot}$ (Abac et al., 2024). In both cases, those components fall into the “mass gap” where they could be the most massive neutron star or the lightest stellar-mass black hole.

Therefore, having more observations of objects with masses belonging to the “mass gap” would resolve the problem of the maximum mass in neutron stars. The PM stage can reveal important information about the mass limit although it is not yet observationally available through current GW detectors, still we can use BNS simulations (e.g., (Gonzalez et al., 2023)) and focus on their PM signals to study the probability of detection of future GW observatories such as Einstein Telescope (ET) (Hild et al., 2011), Cosmic Explorer (CE) (Reitze et al., 2019) and Neutron-star Extreme Matter Observatory (NEMO) (Ackley et al., 2020). By using BNS simulations with total masses in the range $M_T = [2.6 - 3.42] M_{\odot}$ to explore the detectability of next-generation

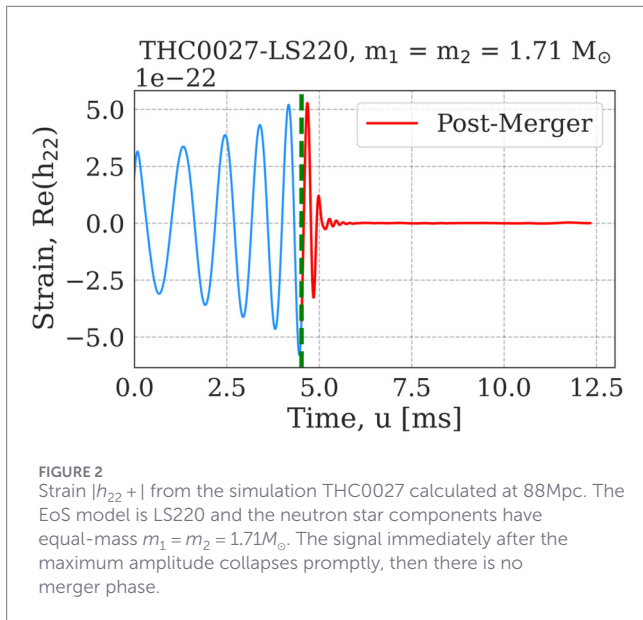
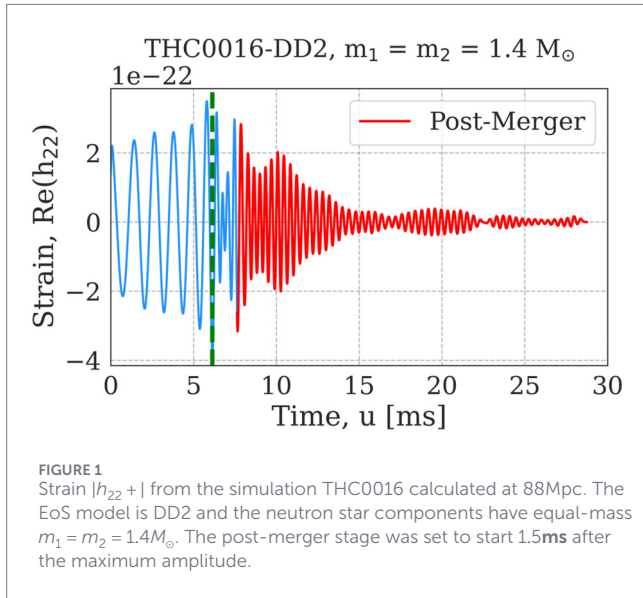
observatories, we set the first steps that will lead us, in a future work, to study the mass precision in the NS maximum mass.

In Section 2, we analyze the probability of detection of ET, CE and NEMO for BNS signals with high values of total mass extracted at distances based on the GW190425 event ($d = [88, 159]$ Mpc). Section 3 will discuss the results and propose a few perspectives.

2 BNS signals and the next-generation of GW detectors

We used a set of BNS simulations from the Computational Relativity (CoRe) database (Collaboration, 2024; Gonzalez et al., 2023) that were characterized as binaries with total gravitational masses such as $M_T = 2.6 M_{\odot}$ up to $M_T = 3.42 M_{\odot}$. We choose different EoS models: SLy (Douchin and Haensel, 2001); BHBlp (Banik et al., 2014); DD2 (Typel et al., 2010); LS220 (Lattimer and Swesty, 1991); SFHo (Steiner et al., 2013), BLQ, BLh (Prakash et al., 2021); SLy4 (Chabanat et al., 1998). The equations of state of these simulations cover different stiffness and matter compositions, which will lead to different possibilities for the product: a prompt-collapse black hole, an intermediate state of HMNS or SMNS before ending as a black hole, or just stabilizing as a new massive neutron star. The neutron star masses of the chosen simulations are in the range of the estimated values of GW190425, and based on this event, the GW strains from the CoRe database were obtained at two luminosity distances: 88 Mpc and 159 Mpc (see Table 2 for details). Since we are focused on the post-merger stage, we separate the signal into three parts: the *inspiral* ends when the maximum amplitude of the (2,2) mode $|h_{22}|$ is achieved. From there, the next phase is the *merger* stage, which is a short transition to the *post-merger* stage. Numerical studies, using the method of the minimum lapse, suggest that the time for a prompt black hole collapse is approximately ≤ 2 ms Kölsch et al. (2022), a similar value is also considered in Agathos et al. (2020). Other groups, based on numerical simulations, set this time as 3 ms (Hotokezaka et al., 2011) and also 1.25 ms (Królak et al., 2023). Therefore, we assume a value of 1.5 ms for this work. This interval represents the fastest merger duration possible, and also indicates the transition to the post-merger stage. Then, when there is no prompt collapse to a black hole as in Figure 1, the post-merger stage begins at 1.5 ms after the maximum amplitude of the inspiral stage. While in a prompt-collapse black hole case, we have no post-merger signal, as can be observed for the simulation THC0027 (see Figure 2), where the waveform damps almost instantly. In principle, the simulations used in this work do not present parameter degeneracy, since each waveform is determined by a specific combination of individual masses, spins, and EoS. These parameters define different gravitational wave signals in both the inspiral and post-merger stages. In practice, the inclusion of spins, magnetic fields, and other physical phenomena produces deviations in the waveforms that cannot be experimentally resolved nowadays, producing in this way a parameter degeneracy; this possible degeneracy does not modify the main conclusions obtained.

We compare the post-merger signals with the sensitivity curves of ET, CE and NEMO which are expressed in terms of the characteristic strain as a function of the frequency.



The detectors considered in this work differ in geometry, arm length, and frequency bands that will define their sensitivity performance for the post-merger stage. Table 1 summarizes their main characteristics based on the reports for the Einstein Telescope ET Steering Committee Editorial Team (2020), the Cosmic Explorer Reitze et al. (2019), and the Neutron-star Extreme Matter Observatory Ackley et al. (2020).

Following the definitions in (Moore et al., 2014), we use the characteristic strain (h_c) defined in Equation 1

$$h_c(f) = 2f|\tilde{h}(f)|, \quad (1)$$

where $\tilde{h}(f)$ is the Fourier transform of the post-merger strain $h_{22}+$.

In order to obtain the signal-to-noise (SNR) we follow the matched-filtering process using the response function of the gravitational-wave detector. The detected strain $h(t)$ is a linear combination of the 2 GW polarizations, multiplied by the

detector’s antenna pattern functions and the inclination of the source: $h(t) = (1/2)(1 + \cos^2 \iota)F_+(\theta, \phi, \psi)h_+(t) + \cos \iota F_\times(\theta, \phi, \psi)h_\times(t)$. Here, $F(\theta, \phi, \psi)$, depends on the position of the source in the sky (θ, ϕ) and the polarization angle ψ . The factors $(1 + \cos^2 \iota)/2$ and $\cos \iota$ depend on the inclination angle ι between the angular momentum of the binary and the line of sight of the detector (Creighton and Anderson, 2011). The total detector output is $O(t) = n(t) + h(t)$, where $n(t)$ is noise that we model as Gaussian and stationary. The SNR for a known template is defined as in Equation 2 (Maggiore, 2007)

$$\rho = 2 \frac{\text{Re} \left\{ \int_0^\infty \frac{df}{S_n(f)} \tilde{O}(f) \tilde{h}_T^*(f) e^{-2\pi i f t_c} \right\}}{\sqrt{\int_0^\infty \frac{df}{S_n(f)} |\tilde{h}_T(f)|^2}}, \quad (2)$$

where $S_g(f)$ is the one-sided power spectral density of the detector noise, $\tilde{h}_T(f)$ is the Fourier transform of the post-merger strain that we call “template” ($h(t) \equiv h_T$), $\tilde{O}(f)$ is the Fourier transform of the output signal and t_c is the arrival time of the signal at the detector, but since we do not know its exact value, we scan possible values for it, maximizing the match between the output signal and the template.

In order to cover all possibilities, we average the SNR over the mentioned 4 angles, each following the distributions: $P(\theta) \propto \sin \theta$ (uniform on the sphere), $P(\iota) \propto \sin \iota$ (uniform), $P(\phi) \propto \text{const}$, $P(\psi) \propto \text{const}$ Creighton and Anderson (2011); Maggiore (2007). This average is approximated by a Monte Carlo sum expressed as in Equation 3

$$\bar{\rho} \approx \frac{1}{N_s} \sum_{i=1}^{N_s} \rho(\theta_i, \phi_i, \psi_i, \iota_i), \quad (3)$$

where $\theta_i, \phi_i, \psi_i, \iota_i$ are random samples according to the mentioned distributions. This ensures that the SNR is not calculated for a particular case, which might be considered a strong assumption.

In Figures 3, 4 we see an example of the characteristic strain of the post-merger phase of two simulations, THC0016 and THC0027, together with the sensitivity curves of the ET, CE and NEMO detectors. However, the averaged SNR for THC0016 shows $\bar{\rho} = 3.00 \pm 1.64$ (ET), $\bar{\rho} = 5.23 \pm 2.84$ (CE) and $\bar{\rho} = 4.26 \pm 2.30$ (NEMO). In the same way, for THC0027 the averaged SNRs are 3.30 ± 1.90 for ET, 4.96 ± 2.84 for CE and 3.05 ± 1.76 for NEMO. See Table 2 for more details on the SNRs and the frequencies of the main peak in the characteristic strain spectra for all post-merger simulations.

The SNR values for the post-merger signals are shown in Table 2 for a luminosity distance of $d = 88$ Mpc and in Table 3 for $d = 159$ Mpc. The further distance results in weaker detections; in any case, none of the chosen simulations satisfies the condition $\text{SNR} \geq 8$.

For better visualization of the SNR values when $d = 88$ Mpc, see Figure 5 where we identify the lowest, highest, mean, and median values for each detector. CE is the detector that obtains the highest $\bar{\rho}_{\text{mean}} = 4.49$. We can see in Figure 6 how the SNR values are spread according to the frequency of the main peak in the characteristic strain. The error bars are considerable as a result of the averaging over all four angles. This highlights the dependence of the SNR on the orientation angles, and as a consequence, only a few of the post-merger simulations barely approach the required threshold $\text{SNR} \geq 8$.

TABLE 1 Main characteristics of the Cosmic Explorer (CE), Einstein Telescope (ET) and Neutron-star Extreme Matter Observatory (NEMO). We show the configuration, the arm length and the frequency band.

Detector	Configuration	Arm length	Frequency-band
CE	2 L-shaped	40 and 20 km	5 Hz to 4 kHz
ET	Underground triangle	10 km	3 Hz to several kHz
NEMO	L-shaped	4 km	≤ 50 Hz to ≥ 1 kHz

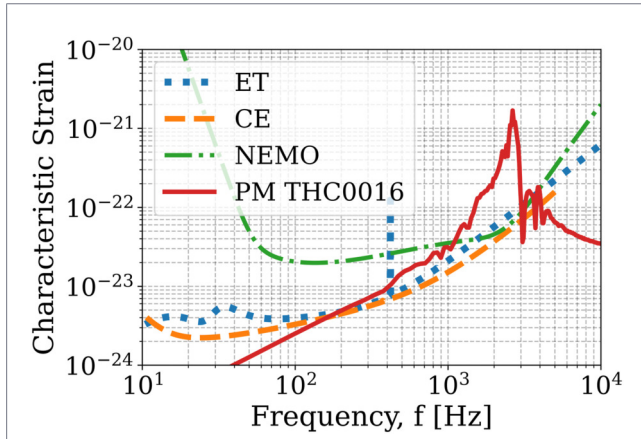


FIGURE 3 An example of a characteristic strain of the THC0016 post-merger signal and the sensitivity curves for ET, CE and NEMO detectors. The main peak of the post-merger signal is at ~2.649kHz.

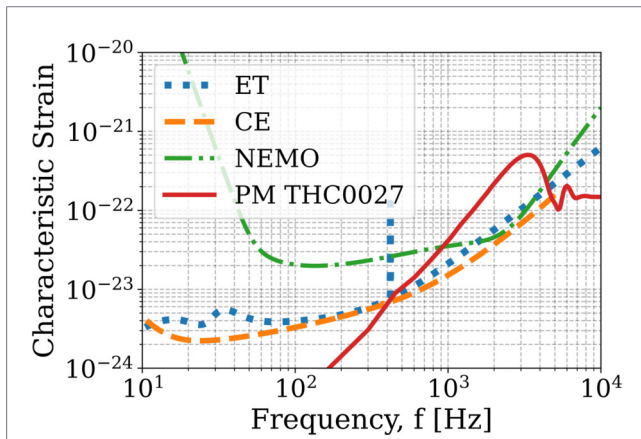


FIGURE 4 An example of a characteristic strain of the THC0027 post-merger signal and the sensitivity curves of the ET, CE, and NEMO. The main peak of the post-merger signal is at ~3.305kHz.

Once we obtain the SNR values, we can estimate the horizon distance for each detector. To include the uncertainty of the SNR, we propagate the errors for each equation using standard error propagation. For this estimate, we adopt the detection threshold of $SNR_{ref} = 8$ for the post-merger signal, based on the work of (Panther and Lasky, 2023), who show that with appropriate noise mitigation, $SNR \geq 8$ is enough for a confident detection of the post-merger signal.

The SNR from matched-filtering is inversely proportional to the luminosity distance $SNR \propto 1/d$, as shown in the discussion about the “sight distance to coalescing binaries” by Maggiore (2007). If we can compare the calculated SNR with the reference SNR_{ref} , we express it as in Equation 4

$$\frac{SNR_i}{SNR_{ref}} \propto \frac{1/d}{1/d_{max}} \propto \frac{d_{max}}{d} \tag{4}$$

Then, the maximum distance to which a source with SNR_i can be detected, given a threshold SNR_{ref} at the source distance d , is Equation 5

$$d_{max} = \frac{SNR_i}{SNR_{ref}} d, \tag{5}$$

where $d = 88$ or 159 Mpc and SNR_i are the SNR values presented in Tables 1,3. For any other threshold, the results can be rescaled, since there is a relation between the maximum distance and the reference SNR as shown in Equation 5.

The proportionality in Equation 4 becomes an equality because we consider the same source; therefore, the constant in $SNR = K/d$ is the same. Now, we do not use all the calculated SNR values because we can choose representative results such as the highest, lowest, and arithmetic mean values, denoted as SNR_{high} , SNR_{low} and SNR_{mean} . These numbers are better identified in Figure 5 for the sources at 88 Mpc, but Table 4 summarizes these representative values for the post-merger simulations located at 88 Mpc and 159 Mpc.

The maximum distance calculated by Equation 5 defines the comoving spherical volume

$$V_c = (4\pi/3) d_{max}^3 \tag{6}$$

within which a number of BNS events N are expected to be detected. Since we are working with distances of 88 Mpc and 159 Mpc for the simulated sources, they belong to very low redshifts, then in a flat Λ CDM cosmology, this d_{max} is the comoving distance that defines the spherical comoving volume V_c as shown in the Euclidean formula, Equation 6.

Based on the merger rate estimates of (LIGO Scientific Collaboration and Virgo Collaboration, 2023), the values R_0 we use for BNS systems are in the range of $10 - 1700 \text{ Gpc}^{-3}\text{yr}^{-1}$ at $z = 0$. Therefore, from a simplified form of the merger rate expressed as in Equation 7 Du et al. (2025).

$$R_0 = \frac{N}{V_c t}, \tag{7}$$

where t is the observing time, we calculate the number of detections N with the Equation 8

$$N = R_0 V_c t. \tag{8}$$

TABLE 2 Binary neutron star simulations assumed to be placed at a luminosity distance of $d = 88\text{Mpc}$. We show the gravitational masses m_1, m_2 , and the total mass $M_T = m_1 + m_2$, all measured in solar masses. The table also displays the frequency of the main peak in the post-merger characteristic strain, h_c , and provides the Monte Carlo averaged signal-to-noise ratio (SNR) for the Einstein Telescope (ET), Cosmic Explorer (CE), and Neutron-star Extreme Matter Observatory (NEMO).

Name	EoS	m_1	m_2	M_T	h_c in kHz	ET SNR	CE SNR	NEMO SNR
THC0005	BHB1p	1.4	1.2	2.6	2.481	2.56 ± 1.39	4.44 ± 2.40	3.64 ± 1.97
THC0009	BHB1p	1.6	1.6	3.2	2.578	3.39 ± 1.96	5.34 ± 3.06	3.40 ± 1.92
THC0016	DD2	1.4	1.4	2.8	2.649	3.00 ± 1.64	5.23 ± 2.84	4.26 ± 2.30
THC0027	LS220	1.71	1.71	3.42	3.305	3.30 ± 1.90	4.96 ± 2.84	3.05 ± 1.76
THC0051	SLy	1.654	1.654	3.308	3.304	2.69 ± 1.59	4.54 ± 2.67	3.18 ± 1.90
THC0062	BLQ	1.6	1.6	3.2	3.027	3.20 ± 1.83	4.77 ± 2.70	2.92 ± 1.64
THC0068	BLQ	1.5	1.5	3.0	2.898	2.61 ± 1.50	4.15 ± 2.37	2.72 ± 1.55
THC0074	SFHo	1.654	1.654	3.308	3.549	2.61 ± 1.54	4.24 ± 2.48	2.77 ± 1.63
THC0095	SLy4	1.452	1.283	2.735	3.496	1.81 ± 0.94	3.12 ± 1.62	2.20 ± 1.14
THC0107	BLh	1.6	1.6	3.2	3.021	2.50 ± 1.49	4.11 ± 2.44	2.79 ± 1.66

TABLE 3 Monte Carlo averaged Signal-to-noise ratio (SNR) for the binary neutron star simulations from Table 2, calculated at a higher luminosity distance, $d = 159\text{Mpc}$.

Name	ET SNR	CE SNR	NEMO SNR
THC0005	1.42 ± 0.77	2.13 ± 1.15	1.75 ± 0.94
THC0009	1.93 ± 1.08	2.56 ± 1.46	1.63 ± 0.92
THC0016	1.66 ± 0.91	2.51 ± 1.36	2.04 ± 1.10
THC0027	1.83 ± 1.05	2.38 ± 1.36	1.46 ± 0.84
THC0051	1.49 ± 0.88	2.18 ± 1.28	1.52 ± 0.91
THC0062	1.77 ± 1.01	2.29 ± 1.29	1.40 ± 0.78
THC0068	1.44 ± 0.83	1.99 ± 1.14	1.30 ± 0.74
THC0074	1.45 ± 0.85	2.03 ± 1.19	1.33 ± 0.78
THC0095	1.00 ± 0.52	1.49 ± 0.78	1.06 ± 0.55
THC0107	1.38 ± 0.82	1.97 ± 1.17	1.34 ± 0.80

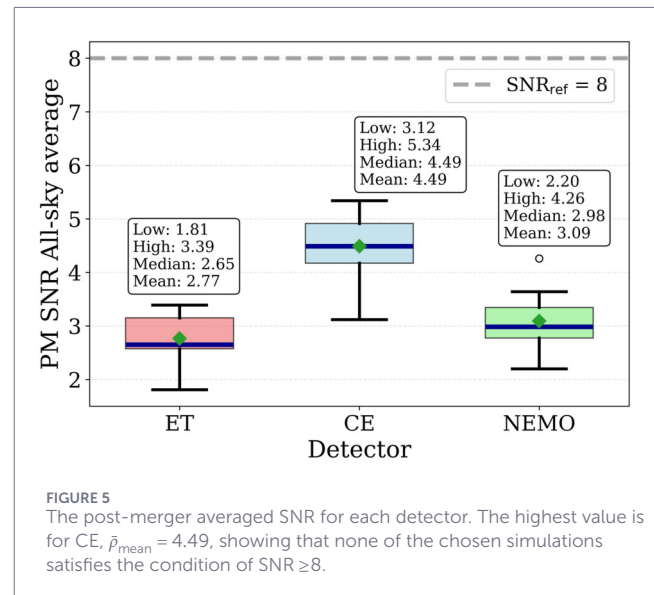


FIGURE 5 The post-merger averaged SNR for each detector. The highest value is for CE, $\bar{p}_{\text{mean}} = 4.49$, showing that none of the chosen simulations satisfies the condition of $\text{SNR} \geq 8$.

In this work, $t = 1\text{yr}$ reports the number of detections per year, and the uncertainty about the number of detections is in terms of the propagated error from V_c , which at the same time contains the error of d_{max} , and this incorporates the SNR error. The distribution of the number of detections is shown in Figures 7, 8. None of the simulations achieves a mean value of $N \geq 1$ per year; this only happens at the upper extreme of the error bar for some cases, especially for the CE detector.

To summarize the final results, we show only representative values for the merger rate: the lower bound ($10\text{Gpc}^{-3}\text{yr}^{-1}$), the upper bound ($1700\text{Gpc}^{-3}\text{yr}^{-1}$), and their midpoint ($850\text{Gpc}^{-3}\text{yr}^{-1}$). The results present in Tables 5,6 show that CE provides $N \geq 1$ for the most optimistic merger rates. While ET and NEMO results remain below 1 detection per year for all the merger rates, except for the highest SNR and merger rate in NEMO.

Recent studies suggest that the BNS merger rate is reduced to $R_0 = 7.6 - 250\text{Gpc}^{-3}\text{yr}^{-1}$ (Abac et al., 2025) and $2.8\text{Gpc}^{-3}\text{yr}^{-1}$

$\leq R_0 \leq 480\text{Gpc}^{-3}\text{yr}^{-1}$ (Salafia, 2025). The lower bound would reduce the number of expected detections, since $N = R_0 V_c t$. However, this would not affect the main conclusion of this work because we do a comparison between detectors, and since they are characterized by fixed sensitivity curves, the CE will still provide the best detectability results compared to the other two detectors.

3 Conclusion

By analyzing the post-merger gravitational wave signals with component masses and distances based on the GW190425 event, that is, binary systems with high values of total mass, we find the possible number of detections per year with next-generation GW detectors. The results show that CE performs better than ET and NEMO, although the uncertainty is considerable due to

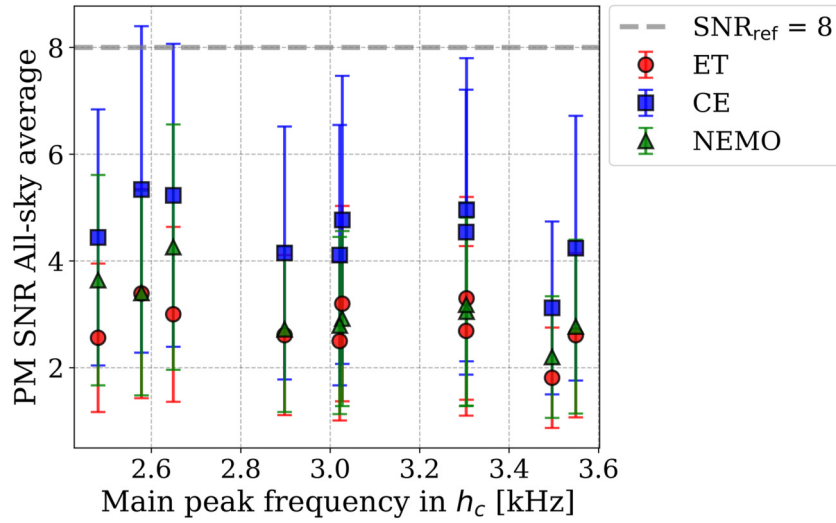


FIGURE 6 The post-merger SNR values and the main peak frequencies in the characteristic strain. No post-merger signals of the chosen simulations are detectable.

TABLE 4 Representative values of the SNR for each detector at both source distances.

Distance	Detector	SNR _{low}	SNR _{mean}	SNR _{high}
88 Mpc	ET	1.81 ± 0.94	2.77 ± 1.58	3.39 ± 1.96
	CE	3.12 ± 1.62	4.49 ± 2.54	5.34 ± 3.06
	NEMO	2.20 ± 1.14	3.09 ± 1.75	4.26 ± 2.30
159 Mpc	ET	1.00 ± 0.52	1.54 ± 0.87	1.93 ± 1.08
	CE	1.49 ± 0.78	2.15 ± 1.22	2.56 ± 1.46
	NEMO	1.06 ± 0.55	1.48 ± 0.84	2.04 ± 1.10

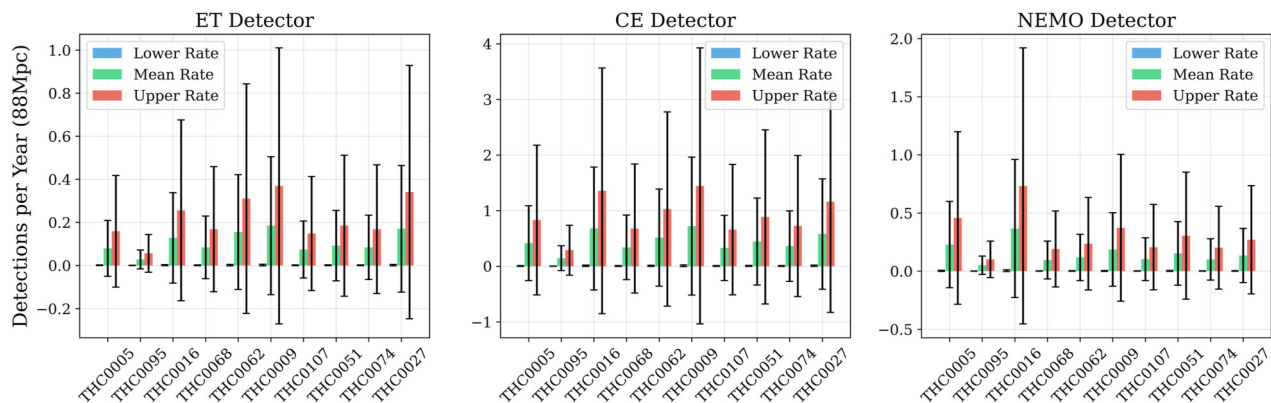


FIGURE 7 Distribution of the number of detections for each simulation when the source is at 88 Mpc. Number of detections $N \geq 1$ are achieved mostly for CE detector and the upper rate $R_0 = 1700 \text{ Gpc}^{-3} \text{ yr}^{-1}$.

averaging the SNR over the four angles or orientation and position of the source relative to the detectors. For example, for the 88 Mpc simulations, the best yearly number of detection achieved by CE is 1.44 ± 2.48 , while ET and NEMO obtain 0.369 ± 0.600 and $0.733 \pm$

1.187 , respectively. The corresponding simulations for the highest SNR is THC0009 with $M_T = 3.2$ and BHBlp as EoS for ET and CE, instead NEMO obtains the highest SNR for THC0016, which has $M_T = 2.8$ and DD2 as EoS. On the other hand, the lowest SNR in the

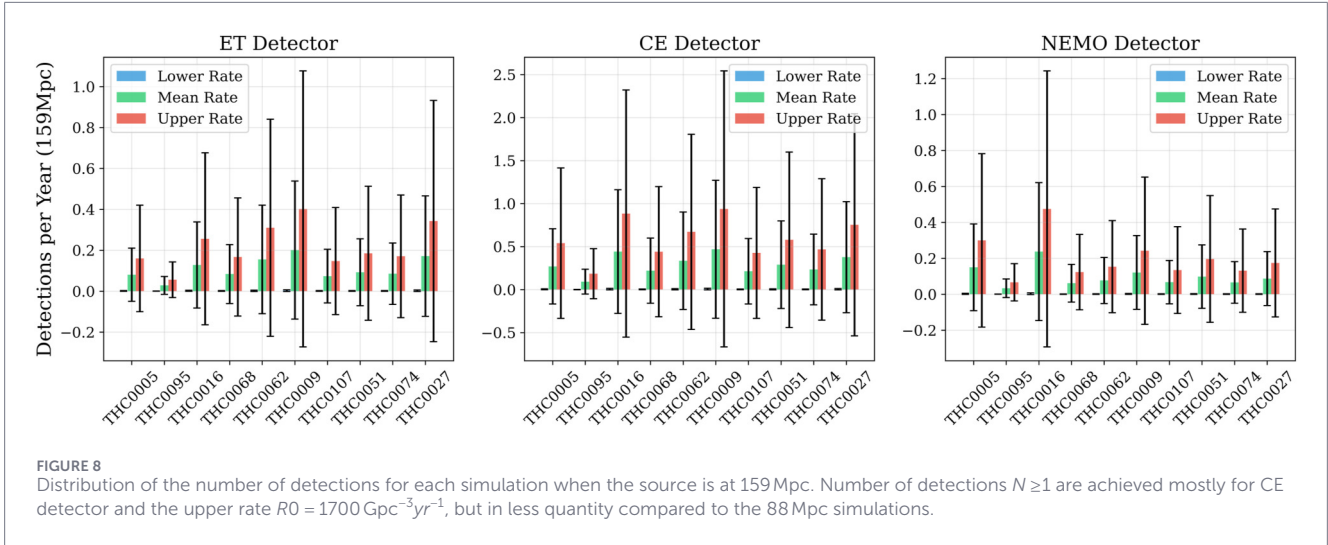


FIGURE 8 Distribution of the number of detections for each simulation when the source is at 159 Mpc. Number of detections $N \geq 1$ are achieved mostly for CE detector and the upper rate $R_0 = 1700 \text{ Gpc}^{-3} \text{ yr}^{-1}$, but in less quantity compared to the 88 Mpc simulations.

TABLE 5 Number of detections per year for the lowest, mean, and highest SNR values from the simulations for each detector at 88 Mpc. The Distance column refers to the horizon distance or d_{max} . Results are shown for three values for the merger rate R_0 .

SNR	Detector	d_{max} (Gpc)	Number of detections		
			$R_0 = 10 \text{ Gpc}^{-3} \text{ yr}^{-1}$	$R_0 = 850 \text{ Gpc}^{-3} \text{ yr}^{-1}$	$R_0 = 1700 \text{ Gpc}^{-3} \text{ yr}^{-1}$
Lowest	ET	0.019 ± 0.010	0.0003 ± 0.0005	0.0281 ± 0.0437	0.0562 ± 0.0875
	CE	0.034 ± 0.017	0.0016 ± 0.0026	0.1439 ± 0.2241	0.2878 ± 0.4483
	NEMO	0.024 ± 0.012	0.0005 ± 0.0009	0.0504 ± 0.0784	0.1009 ± 0.1568
Mean	ET	0.030 ± 0.017	0.0011 ± 0.0020	0.1007 ± 0.1723	0.2014 ± 0.3447
	CE	0.049 ± 0.027	0.0050 ± 0.0008	0.4289 ± 0.7280	0.8579 ± 1.456
	NEMO	0.034 ± 0.019	0.0016 ± 0.0027	0.1398 ± 0.2375	0.2796 ± 0.4751
Highest	ET	0.037 ± 0.021	0.0021 ± 0.0037	0.1846 ± 0.3202	0.3692 ± 0.6004
	CE	0.058 ± 0.033	0.0084 ± 0.0145	0.7216 ± 1.2405	1.443 ± 2.481
	NEMO	0.046 ± 0.025	0.0043 ± 0.0069	0.3663 ± 0.5934	0.7327 ± 1.1868

TABLE 6 Number of detections per year for the lowest, mean, and highest SNR values from the simulations for each detector at 159 Mpc. The Distance column refers to the horizon distance or d_{max} . Results are shown for three values for the merger rate R_0 .

SNR	Detector	d_{max} (Gpc)	Number of detections		
			$R_0 = 10 \text{ Gpc}^{-3} \text{ yr}^{-1}$	$R_0 = 850 \text{ Gpc}^{-3} \text{ yr}^{-1}$	$R_0 = 1700 \text{ Gpc}^{-3} \text{ yr}^{-1}$
Lowest	ET	0.0198 ± 0.010	0.0003 ± 0.0005	0.0279 ± 0.0436	0.0559 ± 0.0872
	CE	0.029 ± 0.015	0.0010 ± 0.0017	0.0924 ± 0.1452	0.1849 ± 0.2904
	NEMO	0.021 ± 0.0109	0.0004 ± 0.0006	0.0332 ± 0.0518	0.0665 ± 0.1036
Mean	ET	0.031 ± 0.017	0.0012 ± 0.0020	0.1020 ± 0.1730	0.2041 ± 0.3460
	CE	0.043 ± 0.024	0.0032 ± 0.0055	0.2778 ± 0.4729	0.5556 ± 0.9458
	NEMO	0.029 ± 0.016	0.0010 ± 0.0018	0.0906 ± 0.1542	0.1812 ± 0.3085
Highest	ET	0.038 ± 0.021	0.0023 ± 0.0039	0.2009 ± 0.3373	0.4019 ± 0.6747
	CE	0.051 ± 0.029	0.0055 ± 0.0094	0.4689 ± 0.8023	0.9379 ± 1.605
	NEMO	0.040 ± 0.022	0.0027 ± 0.0045	0.2373 ± 0.3838	0.4746 ± 0.7677

three detectors corresponds to THC0095 with $M_T = 2.735$ and $SLy4$ as EoS. Most of the simulations we selected for this study have total masses $M_T \geq 3.0 M_\odot$ and the main peak frequencies were around 2.5–3.5 kHz. In this matter, the observation of post-merger signals from high total mass BNS systems is very challenging.

In a future work, we would follow these steps to determine the number of detections and combine it with the remnant mass distribution to study the mass precision in the maximum mass of neutron stars. We should choose other simulations with properties similar to the GW170817 event and test the results for two cases: simulations with different EoS and fixed component mass and simulations with fixed EoS and different masses.

Data availability statement

The raw data supporting the conclusions of this article will be made available by the authors, without undue reservation.

Author contributions

GC-S: Formal Analysis, Methodology, Software, Investigation, Writing – original draft. OA: Project administration, Methodology, Investigation, Funding acquisition, Conceptualization, Writing – review and editing, Formal Analysis, Supervision. HO: Supervision, Writing – review and editing, Investigation. MU: Formal Analysis, Validation, Methodology, Investigation, Software, Supervision, Writing – review and editing.

Funding

The author(s) declared that financial support was received for this work and/or its publication. This work was financially supported by Coordenação de Aperfeiçoamento de Pessoal de Nível Superior - Brasil (CAPES) Finance Code 001 (to Gabriela Conde-Saavedra). Conselho Nacional de Desenvolvimento Científico e Tecnológico (CNPq) and Fundação Carlos Chagas Filho de Amparo à Pesquisa do Estado do Rio de Janeiro (FAPERJ) (Grant No. E-26/200.774/2023 Bolsas de Bancada de Projetos (BBP)) (to H. P. de Oliveira). The Brazilian Ministry of Science, Technology and Innovation and the Brazilian Space Agency (AEB) under PO 20VB.0009, and by CNPq grant number 310087/2021-0 (to Odylio D. Aguiar). CNPq for the Bolsa de Produtividade em Pesquisa (PQ), process number 302954/2025-2 (to Maximiliano Ujevic).

References

- Abac, A. G., Abbott, R., Abouelfettouh, I., Acernese, F., Ackley, K., Adhicy, S., et al. (2024). Observation of gravitational waves from the coalescence of a 2.5–4.5 M_\odot compact object and a neutron star. *Astrophysical J. Lett.* 970, L34. doi:10.3847/2041-8213/ad5beb
- Abac, A. G., et al. (2025). GWTC-4.0: population properties of merging compact binaries. *arXiv preprint arXiv:2508.18083*.

Acknowledgements

This study is part of the PhD Program at the Astrophysics Division of Instituto Nacional de Pesquisas Espaciais, São José dos Campos, Brazil. Gabriela Conde Saavedra is deeply grateful for the financial support given by the Coordenação de Aperfeiçoamento de Pessoal de Nível Superior - Brasil (CAPES) Finance Code 001. H. P. de Oliveira thanks Conselho Nacional de Desenvolvimento Científico e Tecnológico (CNPq) and Fundação Carlos Chagas Filho de Amparo à Pesquisa do Estado do Rio de Janeiro (FAPERJ) (Grant No. E-26/200.774/2023 Bolsas de Bancada de Projetos (BBP)). ODA thanks the Brazilian Ministry of Science, Technology and Innovation and the Brazilian Space Agency (AEB), which supported the present work under PO 20VB.0009. He also thanks CNPq for grant number 310087/2021-0. MU thanks CNPq for the Bolsa de Produtividade em Pesquisa (PQ), process number 302954/2025-2. G. Conde-Saavedra acknowledges Josiel M. Mendonça for providing the matched-filtering code and giving feedback to preliminary results, and to the Gravitational Wave group of the Instituto Nacional de Pesquisas Espaciais (GWINPE) for the discussions during the weekly meetings.

Conflict of interest

The author(s) declared that this work was conducted in the absence of any commercial or financial relationships that could be construed as a potential conflict of interest.

Generative AI statement

The author(s) declared that generative AI was used in the creation of this manuscript. AI was used to generate some of the computer codes.

Any alternative text (alt text) provided alongside figures in this article has been generated by Frontiers with the support of artificial intelligence and reasonable efforts have been made to ensure accuracy, including review by the authors wherever possible. If you identify any issues, please contact us.

Publisher's note

All claims expressed in this article are solely those of the authors and do not necessarily represent those of their affiliated organizations, or those of the publisher, the editors and the reviewers. Any product that may be evaluated in this article, or claim that may be made by its manufacturer, is not guaranteed or endorsed by the publisher.

- Abbott, B. P., Abbott, R., Abbott, T. D., Acernese, F., Ackley, K., Adams, C., et al. (2017). GW170817: observation of gravitational waves from a binary neutron star inspiral. *Phys. Rev. Lett.* 119, 161101. doi:10.1103/PhysRevLett.119.161101

- Abbott, B. P., Abbott, R., Abbott, T. D., Acernese, F., Ackley, K., Adams, C., et al. (2018). GW170817: measurements of neutron star radii and equation of state. *Phys. Rev. Lett.* 121, 161101. doi:10.1103/PhysRevLett.121.161101

- Abbott, B. P., Abbott, R., Abbott, T. D., Acernese, F., Ackley, K., Adams, C., et al. (2019). Properties of the binary neutron star merger GW170817. *Phys. Rev. X* 9, 011001. doi:10.1103/PhysRevX.9.011001
- Abbott, B. P., Abbott, R., Abbott, T. D., Abraham, S., Acernese, F., Ackley, K., et al. (2020a). GW190425: observation of a compact binary coalescence with total mass $\sim 3.4 M_{\odot}$. *Astrophysical J. Lett.* 892, L3. doi:10.3847/2041-8213/ab75f5
- Abbott, R., Abbott, T. D., Abraham, S., Acernese, F., Ackley, K., Adams, C., et al. (2020b). GW190814: gravitational waves from the coalescence of a 23 solar mass Black hole with a 2.6 solar mass compact object. *Astrophysical J. Lett.* 896, L44. doi:10.3847/2041-8213/ab960f
- Ackley, K., Adya, V. B., Agrawal, P., Altin, P., Ashton, G., Bailes, M., et al. (2020). Neutron star extreme matter observatory: a kilohertz-band gravitational-wave detector in the global network. *Publ. Astron. Soc. Aust.* 37, e047. doi:10.1017/pasa.2020.39
- Agathos, M., Zappa, F., Bernuzzi, S., Perego, A., Breschi, M., and Radice, D. (2020). Inferring prompt black-hole formation in neutron star mergers from gravitational-wave data. *Phys. Rev. D* 101, 044006. doi:10.1103/physrevd.101.044006
- Banik, S., Hempel, M., and Bandyopadhyay, D. (2014). New hyperon equations of state for supernovae and neutron stars in density-dependent hadron field theory. *Astrophysical J. Suppl. Ser.* 214, 22. doi:10.1088/0067-0049/214/2/22
- Bauswein, A., Baumgarte, T. W., and Janka, H.-T. (2013). Prompt merger collapse and the maximum mass of neutron stars. *Phys. Rev. Lett.* 111, 131101. doi:10.1103/physrevlett.111.131101
- Bernuzzi, S., Nagar, A., Balmelli, S., Dietrich, T., and Ujevic, M. (2014). Quasiuniversal properties of neutron star mergers. *Phys. Rev. Lett.* 112, 201101. doi:10.1103/PhysRevLett.112.201101
- Chabanat, E., Bonche, P., Haensel, P., Meyer, J., and Schaeffer, R. (1998). A skyrme parametrization from subnuclear to neutron star densities part ii. Nuclei far from stabilities. *Nucl. Phys. A* 635, 231–256. doi:10.1016/s0375-9474(98)00180-8
- Collaboration, C. R. C. (2024). Computational relativity. Available online at: <http://www.computational-relativity.org/> (Accessed August 15, 2024).
- Creighton, J. D. E., and Anderson, W. G. (2011). *Gravitational-wave physics and astronomy: an introduction to theory, experiment and data analysis*. Weinheim, Germany: Wiley VCH. Wiley Series in Cosmology. doi:10.1002/9783527636089
- Cromartie, H. T., Fonseca, E., Ransom, S. M., Demorest, P. B., Arzoumanian, Z., Blumer, H., et al. (2019). Relativistic shapiro delay measurements of an extremely massive millisecond pulsar. *Nat. Astron.* 4, 72–76. doi:10.1038/s41550-019-0880-2
- Demorest, P. B., Pennucci, T., Ransom, S. M., Roberts, M. S. E., and Hessels, J. W. T. (2010). A two-solar-mass neutron star measured using shapiro delay. *Nature* 467, 1081–1083. doi:10.1038/nature09466
- Dietrich, T., Hinderer, T., and Samajdar, A. (2021). Interpreting binary neutron star mergers: describing the binary neutron star dynamics, modelling gravitational waveforms, and analyzing detections. *General Relativ. Gravit.* 53, 27. doi:10.1007/s10714-020-02751-6
- Douchin, F., and Haensel, P. (2001). A unified equation of state of dense matter and neutron star structure. *Astronomy & Astrophysics* 380, 151–167. doi:10.1051/0004-6361:20011402
- Du, Y. F., Yorgancıoglu, E. S., Yi, S. X., Cao, T. Y., and Zhang, S. N. (2025). A systematic study of binary neutron star merger rate density history using simulated gravitational wave and short gamma-ray burst observations. *Mon. Notices R. Astronomical Soc.* 541, 798–805. doi:10.1093/mnras/staf1043
- ET Steering Committee Editorial Team (2020). Design report update for the einstein telescope. *Tech. Rep. ET-0007B-20, Eur. Gravitational Obs. (EGO)*.
- Farr, W. M., Sravan, N., Cantrell, A., Kreidberg, L., Bailyn, C. D., Mandel, I., et al. (2011). The mass distribution of stellar-mass Black holes. *Astrophysical J.* 741, 103. doi:10.1088/0004-637x/741/2/103
- Gonzalez, A., Zappa, F., Breschi, M., Bernuzzi, S., Radice, D., Adhikari, A., et al. (2023). Second release of the CoRe database of binary neutron star merger waveforms. *Class. Quantum Gravity* 40, 085011. doi:10.1088/1361-6382/acc231
- Hild, S., Abernathy, M., Acernese, F., Amaro-Seoane, P., Andersson, N., Arun, K., et al. (2011). Sensitivity studies for third-generation gravitational wave observatories. *Class. Quantum Gravity* 28, 094013. doi:10.1088/0264-9381/28/9/094013
- Hotokozaka, K., Kyutoku, K., Okawa, H., Shibata, M., and Kiuchi, K. (2011). Binary neutron star mergers: dependence on the nuclear equation of state. *Phys. Rev. D* 83, 124008. doi:10.1103/PhysRevD.83.124008
- Hotokozaka, K., Kiuchi, K., Kyutoku, K., Okawa, H., Sekiguchi, Y.-i., Shibata, M., et al. (2013). Mass ejection from the merger of binary neutron stars. *Phys. Rev. D* 87, 024001. doi:10.1103/physrevd.87.024001
- Kiuchi, K., Cerdá-Durán, P., Kyutoku, K., Sekiguchi, Y., and Shibata, M. (2015). Efficient magnetic-field amplification due to the kelvin-helmholtz instability in binary neutron star mergers. *Phys. Rev. D* 92. doi:10.1103/physrevd.92.124034
- Kölsch, M., Dietrich, T., Ujevic, M., and Bruegmann, B. (2022). Investigating the mass-ratio dependence of the prompt-collapse threshold with numerical-relativity simulations. *Phys. Rev. D* 106, 044026. doi:10.1103/PhysRevD.106.044026
- Królak, A., Jaranowski, P., Bejger, M., Ciecielag, P., Dorosh, O., and Pisanski, A. (2023). Search for postmerger gravitational waves from binary neutron star mergers using a matched-filtering statistic. *Class. Quantum Gravity* 40, 215008. doi:10.1088/1361-6382/acfa5d
- Lattimer, J. M., and Swesty, F. D. (1991). A generalized equation of state for hot, dense matter. *Nucl. Phys. A* 535, 331–376. doi:10.1016/0375-9474(91)90452-C
- LIGO Scientific Collaboration and Virgo Collaboration (2023). Population of merging compact binaries inferred using gravitational waves through GWTC-3. *Phys. Rev. X* 13. doi:10.1103/physrevx.13.011048
- Maggiore, M. (2007). “Gravitational waves,” in *Theory and experiments*, 1. Oxford University Press. doi:10.1093/acprof:oso/9780198570745.001.0001
- Moore, C. J., Cole, R. H., and Berry, C. P. L. (2014). Gravitational-wave sensitivity curves. *Class. Quantum Gravity* 32, 015014. doi:10.1088/0264-9381/32/1/015014
- Özel, F., and Freire, P. (2016). Masses, radii, and the equation of state of neutron stars. *Annu. Rev. Astronomy Astrophysics* 54, 401–440. doi:10.1146/annurev-astro-081915-023322
- Özel, F., Psaltis, D., Narayan, R., and McClintock, J. E. (2010). The Black hole mass distribution in the galaxy. *Astrophysical J.* 725, 1918. doi:10.1088/0004-637X/725/2/1918
- Panther, F. H., and Lasky, P. D. (2023). The effect of noise artefacts on gravitational-wave searches for neutron star post-merger remnants. *Mon. Notices R. Astronomical Soc.* 523, 2928–2933. doi:10.1093/mnras/stad1556
- Perego, A., Rosswog, S., Cabezón, R. M., Korobkin, O., Kappeli, R., Arcones, A., et al. (2014). Neutrino-driven winds from neutron star merger remnants. *Mon. Notices R. Astronomical Soc.* 443, 3134–3156. doi:10.1093/mnras/stu1352
- Prakash, A., Radice, D., Logoteta, D., Perego, A., Nedora, V., Bombaci, I., et al. (2021). Signatures of deconfined quark phases in binary neutron star mergers. *Phys. Rev. D* 104, 083029. doi:10.1103/physrevd.104.083029
- Puecher, A., Dietrich, T., Tsang, K. W., Kalaghatgi, C., Roy, S., Setyawati, Y., et al. (2023). Unraveling information about supranuclear-dense matter from the complete binary neutron star coalescence process using future gravitational-wave detector networks. *Phys. Rev. D* 107, 124009. doi:10.1103/physrevd.107.124009
- Radice, D., Perego, A., Hotokozaka, K., Bernuzzi, S., Fromm, S. A., and Roberts, L. F. (2018). Viscous-dynamical ejecta from binary neutron star mergers. *Astrophysical J. Lett.* 869, L35. doi:10.3847/2041-8213/aaf053
- Radice, D., Bernuzzi, S., and Perego, A. (2020). The dynamics of binary neutron star mergers and their remnants. *Ann. Rev. Nucl. Part. Sci.* 70, 95–119. doi:10.1146/annurev-nucl-013120-114541
- Read, J. S., Baiotti, L., Creighton, J. D. E., Friedman, J. L., Giacomazzo, B., Kyutoku, K., et al. (2013). Matter effects on binary neutron star waveforms. *Phys. Rev. D* 88, 044042. doi:10.1103/physrevd.88.044042
- Reitze, D., Adhikari, R. X., Ballmer, S., Barish, B., Barsotti, L., Billingsley, G., et al. (2019). Cosmic explorer: the U.S. contribution to gravitational-wave astronomy beyond LIGO. *Bull. Am. Astron. Soc.* 51, 035. doi:10.48550/arXiv.1907.04833
- Salafia, O. S. (2025). Detection probability of light compact binary mergers in future observing runs of the current ground-based gravitational wave detector network. *Astron. Astrophys.* 702, A54. doi:10.1051/0004-6361/202555997
- Shibata, M., Zhou, E., Kiuchi, K., and Fujibayashi, S. (2019). Constraint on the maximum mass of neutron stars using GW170817 event. *Phys. Rev. D* 100, 023015. doi:10.1103/physrevd.100.023015
- Steiner, A. W., Hempel, M., and Fischer, T. (2013). Core-collapse supernova equations of state based on neutron star observations. *Astrophysical J.* 774, 17. doi:10.1088/0004-637x/774/1/17
- Takami, K., Rezzolla, L., and Baiotti, L. (2014). Constraining the equation of state of neutron stars from binary mergers. *Phys. Rev. Lett.* 113, 091104. doi:10.1103/physrevlett.113.091104
- Thompson, T. A., Kochanek, C. S., Stanek, K. Z., Dong, S., Drout, M. R., Shappee, B. J., et al. (2019). A noninteracting low-mass Black hole–giant star binary system. *Science* 366, 637–640. doi:10.1126/science.aau4005
- Thorsett, S. E., and Chakrabarty, D. (1999). Neutron star mass measurements. I. Radio pulsars. *Astrophysical J.* 512, 288–299. doi:10.1086/306742
- Typel, S., Röpke, G., Klähn, T., Blaschke, D., and Wolter, H. H. (2010). Composition and thermodynamics of nuclear matter with light clusters. *Phys. Rev. C* 81. doi:10.1103/physrevc.81.015803
- Zhang, C. M., Wang, J., Zhao, Y. H., Yin, H. X., Song, L. M., Menezes, D. P., et al. (2011). Study of measured pulsar masses and their possible conclusions. *Astronomy Astrophysics* 527, A83. doi:10.1051/0004-6361/201015532